frontiers | Frontiers in Earth Science

TYPE Original Research
PUBLISHED 02 February 2023
DOI 10.3389/feart.2023.1059869

OPEN ACCESS

EDITED BY
Xiaomin Xie,
Yangtze University, China

REVIEWED BY
Wei Dang,
Xi'an Shiyou University, China
Yanyan Chen,
Research Institute of Petroleum Exploration and Development (RIPED), China

*CORRESPONDENCE
Kun Jiao,
jiaokun@foxmail.com

SPECIALTY SECTION
This article was submitted to Geochemistry, a section of the journal Frontiers in Earth Science

RECEIVED 02 October 2022
ACCEPTED 10 January 2023
PUBLISHED 02 February 2023

CITATION
Xie G, Jiao K, Deng B, Hao W and Liu S (2023), Pore characteristics and preservation mechanism of over-6000-m ultra-deep shale reservoir in the Sichuan Basin.
Front. Earth Sci. 11:1059869.
doi: 10.3389/feart.2023.1059869

Pore characteristics and preservation mechanism of over-6000-m ultra-deep shale reservoir in the Sichuan Basin

Guoliang Xie[1,2], Kun Jiao[2]*, Bin Deng[2], Weiduo Hao[3,4] and Shugen Liu[2,5]

[1]School of Civil Engineering and Architechure, Tongling University, Tongling, China, [2]State Key Laboratory of Oil and Gas Reservoir Geology and Exploitation, Chengdu University of Technology, Chengdu, China, [3]Department of Earth and Atmospheric Sciences, University of Alberta, Edmonton, AB, Canada, [4]Department of Geology, Northwest University, Xi'an, China, [5]Xihua University, Chengdu, China

Investigation of pore characteristics and their preservation mechanism of over 6000 m ultra-deep shale reservoirs is of significance for shale gas exploration and development in the Sichuan Basin. In this study, the pores structure and multifractal characteristics of pores for the Longmaxi shale and Qiongzhusi shale in the Sichuan Basin are well studied by using field emission scanning electron microscopy (FE-SEM), gas adsorption and multifractal analysis. The results show that: (1) Extremely strong mechanical compaction resulting from ultra-deep burial depth can lead to the homogenization of pore structure, which is characterized by the change of bubble-like OM pores to silt or fracture shape pores and the higher average pore diameter (APD) value. (2) The Longmaxi shale and Qiongzhusi shale reservoirs have the obvious multifractal nature for different pore sizes. Samples from the Longmaxi shale and Qiongzhusi shale in well CS#1 demonstrate the higher average H values and smaller average ΔD values compared with those samples in well MS#1, indicating that shale reservoir in over-pressure condition has higher connectivity and less heterogeneity. The pore preservation in over 6000 m ultra-deep shale reservoirs are influenced by several geological factors, including 1) quartz is beneficial for the preservation of pores especially for OM pores due to its supporting effect; 2) the shale reservoirs in over-pressure show many more OM pores and higher surface porosity than those in normal pressure; 3) the direct floor of Qiongzhusi shale is likely the critical geological factor affecting the pores preservation. Therefore, the Longmaxi shale with both over-pressure condition and high quartz content is likely the best target zone for deep shale gas exploration in the Sichuan Basin.

KEYWORDS

shale gas, pore characteristics, over-pressure, multifractal analysis, preservation mechanism, ultra-deep shale reservoir

Introduction

Recently, great progress in shale gas exploration and development has been made in China, especially in revealing the mechanisms of shale gas generation and accumulation (Guo and Zhang., 2014; Borjigin et al., 2017; Guo et al., 2017; Wang et al., 2019; Shu et al., 2020; Xi et al., 2022), the formation and preservation of organic matter (OM) pores in shales (Liang et al., 2017; Dong et al., 2021; Ma et al., 2022; Teng et al., 2022; Yu K et al., 2022), and the characteristics of shale gas in China (Zou et al., 2010; Zou et al., 2016; Zou et al., 2019; Li et al.,

2021; Feng et al., 2022; Nie et al., 2022). Shale gas production in China exceeded 230×10^8 m^3 by the end of 2021, most of which was distributed in marine Longmaxi shale reservoirs in the Sichuan Basin and its surrounding area. Deep-shale gas with a buried depth of more than 3500 m has become an important potential resource for further shale gas exploration in the Sichuan Basin. He et al. calculated that the distribution area (12.6×10^4 km^2) of the Longmaxi shales with burial depth exceeding 3500 m in the Sichuan Basin is more than twice as large as those with burial depth less than 3500 m (He et al., 2021). The Longmaxi shale with burial depth ranging from 3500 to 4500 m in the southern Sichuan Basin covers an area of about 8.37×10^{12} m^3 (Liu et al., 2021a). Deep shale gas in the Sichuan Basin has displayed a huge potential; for example, the test production of shale gas in well L203 and platform W204 (four sub-wells) reaches 138×10^4 m^3/d and 214.4×10^4 m^3/d, respectively. Moreover, progress has been made in porosity evolution of deep gas shale reservoirs and the enrichment characteristics of deep shale gas. For instance, laminated organic-rich siliceous shale and laminated organic-rich mixed shale of deep shale reservoirs have better shale gas resource potential due to their abundant OM pores (Wang et al., 2022), and OM pores appear to be well preserved in deep shale reservoirs with TOC less than 5.5% (Gao et al., 2022; Zheng et al., 2022). However, the pore characteristics and preservation mechanism of ultra-deep (over 6000 m) shale reservoirs remain unclear.

The pore structure of shale reservoirs is the key factor affecting the transportation and storage properties of shales, further controlling shale gas content (Loucks et al., 2012; Gou et al., 2019; Zheng et al., 2022). Pore size can be divided into micropore (<2 nm), mesopore (2–50 nm), and macropore (>50 nm) (Sing et al., 1985). To evaluate the pore characteristics of shale reservoirs, a series of quantitative methods—such as high-pressure Hg intrusion and low-pressure N_2, CO_2, and Ar gas adsorption (Loucks et al., 2012; Zhang et al., 2017; Zheng et al., 2022)—and visual qualitative methods such as field emission scanning electron microscopy (FE-SEM) and CT have been widely used to obtain information about pores, including porosity, specific surface area (SSA), pore volume (PV), and pore size distribution (PSD), and to provide a visual of pore geometries and distribution (Mastalerz et al., 2013; Yu Y. X et al., 2022; Zheng et al., 2022).

In recent years, a series of ultra-deep wells has been drilled in the Sichuan Basin, for example, well MS#1 (total vertical depth 8418 m) and well CS#1 (total vertical depth 8448 m). These two wells provide an unparalleled opportunity to study the pore characteristics of over- 6000-m ultra-deep shale reservoirs. Huang et al. (2020) reported that formation temperature becomes dominant in over-3200-m shale reservoirs. In other words, the gas adsorption capacity in over-6000-m ultra-deep buried shale reservoirs will decrease significantly due to the high formation temperature. The term "ultra-deep" refers to strata deeper than 25,000 feet (approximately 4572 m), which were widely used in deep continental drilling programs in the last century (Dyman et al., 2003).

In this study, FE-SEM, SEM image processing, and low-pressure CO_2 and N_2 adsorption were used to investigate the pore characteristics of over-6000-m ultra-deep shale reservoirs. Moreover, multifractal analysis was performed to study pore connectivity and heterogeneity and their controlling factors. Finally, we concluded by studying the preservation mechanism of OM pores in over-6000-m ultra-deep shale reservoirs.

Materials and methods

Sampling

Ultra-deep shale samples, including those from Lower Cambrian Qiongzhusi and Lower Silurian Longmaxi shale, were collected from well MS#1 and well CS#1 in the Sichuan Basin. Well MS#1 was drilled on the structural high part of the Malubei anticline within the Tongnanba tectonic belt in the northeastern Sichuan Basin (Figure 1). Thirty-two shale samples from the Longmaxi Formation (6601–6926 m) and Qiongzhusi Formation (7690–8044 m) were collected from well MS#1, with their paleo-burial depths exceeding 8000 m and 11,000 m, respectively (Jiao et al., 2018). The lithology of the Longmaxi shale in well MS#1 consists of gray and dark gray shale with TOC ranging from 0.36% to 4.22% (average 1.32%) and ER_o ranging from 1.77% to 2.17% (average 1.98%). The ER_o refers to the equivalent vitrinite reflectance that is converted from the bitumen reflectance (BR_o) using the formula $ER_o=0.4+0.618\times BR_o$ (Feng, 1988). The lithology of the Qiongzhusi Formation comprises light gray to dark gray silty shale, dark gray shale, and carbonaceous shale with TOC ranging from 0.4% to 8.95% (average 3.25%) and ER_o ranging from 3.05% to 3.27% (average 3.15%).

Well CS#1 is located on the Boya nose structure in the northern slope of the central Sichuan uplift in the northern Sichuan Basin (Figure 1). Thirty shale samples from the Longmaxi Formation (6940–7152 m) and Qiongzhusi Formation (7719–8146 m) were collected from this well, with paleo-burial depths exceeding 9000 m and 12,000 m (Xie, 2020). The Longmaxi shale consists of dark gray and black carbonaceous shale with TOC ranging from 2.05% to 4.38% (average 3.56%) and ER_o ranging from 2.09% to 2.14% (average 2.11%). The Qiongzhusi shale mainly comprises gray and carbonaceous shale with TOC ranging from 0.42% to 4.13% (average 2.0%) and ER_o ranging from 2.08% to 2.22% (average 2.15%). To the best of our knowledge, wells MS#1 and CS#1 are among the deepest boreholes exposing the Cambrian Qiongzhusi Formation and Silurian Longmaxi Formation in Asia, and they provide important information about the pore characteristics of over-6000-m ultra-deep shale reservoirs.

In this study, a total of 62 samples with burial depths exceeding 6000 m were collected. The TOC, ER_o, and mineral composition of these shales are shown in Supplementary Table S1. It is noted that the relatively low value of ER_o for the shales from well CS#1, compared with those from well MS#1, are due to the low geothermal value of the western Sichuan depression (Richardson et al., 2008; Zhu et al., 2015).

Methods

In total, 8–10 large fragments from each cutting sample were selected for optical microscopic and FE-SEM observation. The remaining smaller fragments of samples were ground to 40–60 mesh with an agate mortar. Then, 2 g of 40–60 mesh samples were weighed for low-pressure CO_2 and N_2 adsorption. The remaining samples were ground to less than 200 mesh for XRD and organic geochemistry analysis. TOC and XRD tests were conducted using the LECO C230 Elemental Analyzer and D8 Advance X-ray diffractometer, respectively.

10.3389/feart.2023.1059869

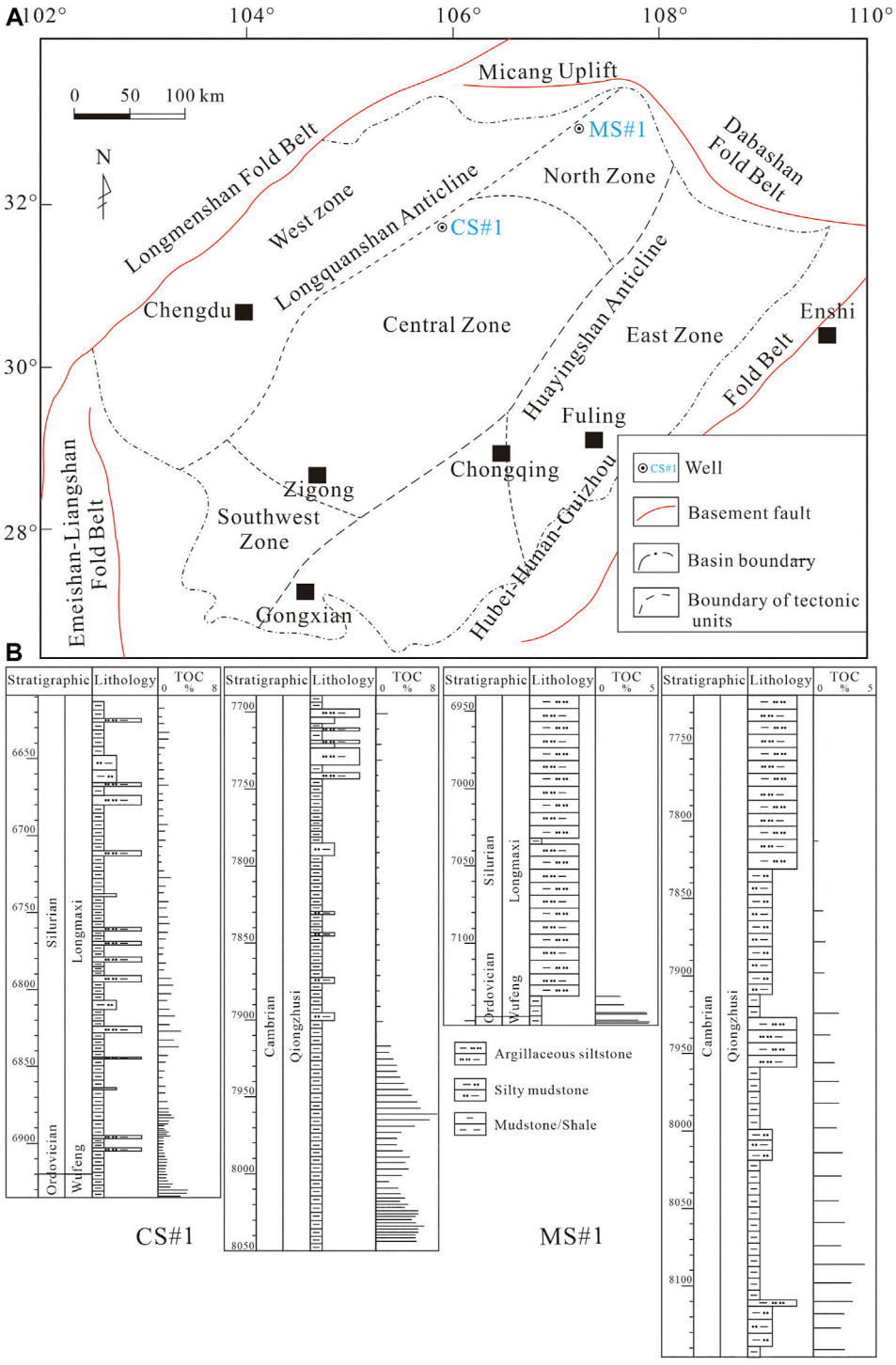

FIGURE 1
Structural units of Sichuan Basin and the studied wells' locations.

FE-SEM observation

Three samples from well MS#1 and seven samples from well CS#1 were selected for SEM observation. Each sample was cut to a size of 8×8×3 mm^3 and wet-polished with ultrathin emery papers with a sequence of 30 μm, 15 μm, 9 μm, 6 μm, 3 μm, and 1 μm to decrease the surface roughness for better performance in argon ion milling. FE-SEM observation was conducted on a Hitachi su8220 scanning electron microscope. Before observation, the surface of sample was coated with a layer of platinum. In total, 80–100 SEM images for each sample were obtained at magnifications varying from 1k× to 200k×. Then, these images were processed with Pores (Particles) and Cracks Analysis System (PCAS) software to acquire quantitative information about the

pores, including their morphological and statistical parameters. The details of the processing procedures for the PCAS can be found in Liu et al. (2011) and Jiao et al. (2018).

CO_2 and N_2 adsorption

Combined low-pressure CO_2 and N_2 adsorption can accurately quantify pore structure over the nanopore range (0.33–100 nm) (Zhang et al., 2017). Samples were degassed at 110°C for 8 hours under vacuum to remove residual moisture and volatile matter before testing (Mastalerz et al., 2013). Low-pressure CO_2 adsorption was performed using ASAP 2020 at 273 K under a relative pressure (P/P_0) ranging from 0.0004 to 0.03. The density functional theory (DFT) method was used to obtain information about pores, including the SSA, PV, and PSD. In fact, the actual detectable pore size ranges approximately from 0.03 to 0.9 nm using the DFT model (Zhang et al., 2017; Jiao et al., 2018).

N_2 adsorption is an efficient method for acquiring pore parameters across the overall nanopore range (0.33–100 nm) (Thommes et al., 2006; Sun et al., 2016; Zhang et al., 2017). The DFT model was performed to provide more accurate information about pore sizes ranging from approximately 0.9 nm to 30 nm (Jiao et al., 2018).

Multifractal analysis

Multifractal theory was first proposed by Mandelbrot to study turbulent flow and was then used to characterize the pore connectivity and heterogeneity of soil and shale (Paz Ferreiro et al., 2010; Paz Ferreiro et al., 2013; Liu et al., 2019). The data sets measured by N_2 or CO_2 adsorption were studied by multifractal analysis using the box counting method (Halsey et al., 1986). The box counting method was applied to CO_2 or N_2 adsorption data to study multifractal characteristics (Lopes and Betrouni, 2009). To implement multifractal analysis for pores of shale, a set of boxes with equal length ε are divided. The boxes are defined as index i, and $N(\varepsilon)$ represents the total number of boxes (size ε) that cover the PSD curve. Thus, the ith box of size ε is specified as ui (ε). For the N_2 or CO_2 adsorption isotherm, the relative pressure P/P_o was taken as the length ε. The probability mass function for the ith box can be calculated as

$$p_i(\varepsilon) = N_i(\varepsilon)/N_T, \tag{1}$$

where $N_i(\varepsilon)$ refers to the volume of adsorbed N_2 or CO_2 for the ith box and $N_i(\varepsilon)$ represents the total volume of adsorbed Ar. $P_i(\varepsilon)$ is defined by an exponential function for each box of size ε as

$$Pi(\varepsilon) \sim \varepsilon^{a}, \tag{2}$$

where a_i represents the singularity exponent that represents how singularities of the system tend to be infinite as ε approaches 0 (Halsey et al., 1986). For multifractal distribution properties of sections of size ε, $N(\varepsilon)$ shows an increase with decreasing ε, following a power law function:

$$N_a(\varepsilon) \sim \varepsilon^{-f(a)}, \tag{3}$$

where $N_a(\varepsilon)$ represents the number of boxes for the probability mass function of the ith box, and $P_i(\varepsilon)$, which has singularity strength between α and $\alpha+d\alpha$. $f(a)$ is the spectrum of the fractal dimension that characterizes abundance in the set with α singularity. $a(q)$ and $f(a)$ are calculated based on the following formula (Chhabra and Jensen, 1989):

$$\mathrm{a}(q) \propto \frac{\sum_{i=1}^{N(\varepsilon)} u_i(q,\varepsilon)\log[p_i(\varepsilon)]}{\log(\varepsilon)}, \tag{4}$$

$$f[a(q)] \propto \frac{\sum_{i=1}^{N(\varepsilon)} \mu_i(q,\varepsilon)\log[\mu_i(q,\varepsilon)]}{\log(\varepsilon)}, \tag{5}$$

where

$$u_i(q,\varepsilon) = \frac{p_i(\varepsilon)^q}{\sum_{i=1}^{N(\varepsilon)} p_i(\varepsilon)^q}. \tag{6}$$

Here, q refers to the exponent that characterizes the fractal properties at different scales of the pore size. a and $f(a)$ can be calculated by linear regression using Formulas (4), (5), whereas q varies from −5 to 5 for successive unit steps. For multifractal theory, the probability distribution function is defined as

$$u(q,\varepsilon) = \sum_{i=1}^{N(\varepsilon)} P_i(\varepsilon)^q \sim \varepsilon^{\tau(q)}, \tag{7}$$

where τ_q refers to the mass scaling function of order q and can be calculated as

$$\tau(q) = \lim_{\varepsilon \to 0} \left[\ln \sum_i P_i(\varepsilon)^q \Big/ \ln(1/\varepsilon)\right]. \tag{8}$$

The generalized dimension (D_q) can be calculated as (Halsey, et al., 1986)

$$D_q = \tau_q \Big/ (q-1), \tag{9}$$

where for q=1, D_q can be expressed as

$$D_1 = \lim_{\varepsilon \to 0} \left(\sum_{i=1}^{N(\varepsilon)} p_i(\varepsilon) \ln p_i(\varepsilon) \Big/ \ln(\varepsilon) \right). \tag{10}$$

The association of D_q and q can reflect the fractal characteristics. ΔD is calculated as $(D_q)_{max}$ - $(D_q)_{min}$, which can be used to characterize the heterogeneity of porosity distribution over the pore size range. The H value, calculated as $(D_2+1)/2$, is known as the Hurst exponent (Holmes et al., 2017). H exponent, ranging from 0.5 to 1, reflects the degree of the positive auto-correlation. Therefore, H can be applied to characterize the pore connectivity and permeability of shales (Martínez et al., 2010). A low H value represents poor pore connectivity.

Results

SEM analysis and PCAS processing

About 1000 SEM images were processed using PCAS analysis. The geometric parameters of pores (e.g., perimeter, area, length, and width) and the statistical parameters of pore systems (e.g., form factor and probability entropy) were obtained through PCAS processing. The form factor refers to the regularity of pores; a value of 1.0 refers to a perfect circle whereas a value of 0.785 represents a square in 2D. A high form factor value indicates complexity in the pore boundary. Probability entropy can describe a pore's directionality in 2D, the value of which ranges from 0 to 1. Pores

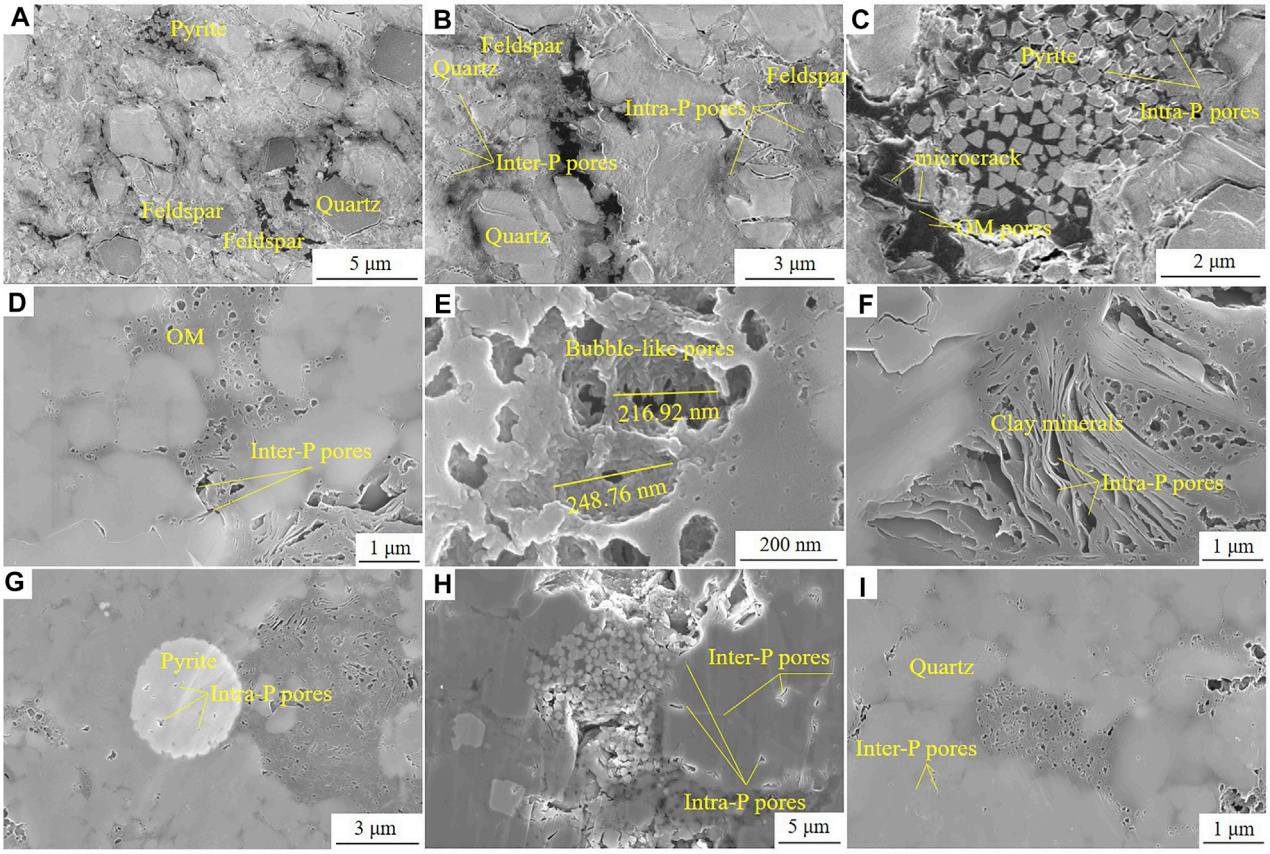

FIGURE 2
Pore types in the Longmaxi and Qiongzhusi shales from wells MS#1 and CS#1. **(A,B)** OM is closely associated with minerals like pyrite and quartz; **(C)** OM is developed within pyrite; **(D)** OM pores; **(E)** bubble-like OM pores; **(F)** OM pores developed in clay minerals; **(G)** intra-P pores developed in pyrite; **(H)** inter-P pores and intra-P pores; **(I)** intra-P pores within quartz.

tend toward the same direction with decreasing values of probability entropy (Soroushian and Elzafraney, 2005). The definition of form factor and probability entropy can be seen in Liu et al. (2011) and Jiao et al. (2018).

Pores can be divided into organic matter (OM) pores and mineral-associated pores, including intraparticle (intra-P) and interparticle (inter-P) pores, based on the pore classification by Loucks et al. (2012). The dimension of OM usually ranges from tens of nanometers to tens of micrometers in the Longmaxi and Qiongzhusi shale from well MS#1 (Figure 2). Most OM particles are crushed and show irregular shapes. OM usually occurs in association with minerals like pyrite (Figure 2A) and quartz (Figure 2B). In general, pores resulting from hydrocarbon generation are often circular or elliptical in shape (Loucks et al., 2009). Figure 2C shows that very few pores are observed in the Longmaxi and Qiongzhusi shale from well MS#1 and that these pores are irregular, silt-like, and microcrack in shape. Intra-P pores occur mainly as intercrystalline pores within pyrite framboid (Figure 2C) and can also develop in quartz (Figure 2B). Moreover, many intra-P pores can be observed within feldspar (Figure 2B), and these are known as dissolved pores. Inter-P pores can be observed between the boundary of quartz and feldspar or other minerals like pyrite (Figure 2B). Mineral-associated pores, including inter-P pores and intra-P pores, contribute up to 95% of the total surface porosity of the shales from well MS#1, based on PCAS analysis (Table 1). Table 1 shows that the mean size of OM pores is 75 nm, whereas the mean size of mineral-associated pores is close to 110 nm. Moreover, the probability entropies of OM and mineral-associated pores are relatively high in all cases, with average values ranging from 0.813 to 0.956, implying that the mineral-associated and OM pores in samples from well MS#1 are more directional. In addition, the higher form factor value of the OM pores demonstrates that OM pores are more regular than mineral-associated pores.

OM pores are very common in the Longmaxi and Qiongzhusi shale from well CS#1. The dimensions of OM particles range from hundreds of nanometers to tens of micrometers (Figure 2D). OM pores in these shales are generally bubble-like in shape and can be up to 50–250 nm (Figures 2D, E). Intra-P pores within clay minerals (Figure 2F) and pyrites (Figure 2G) are dominant, whereas inter-P pores are mainly developed between OM and quartz (Figure 2D) and/or between quartz (Figure 2H). Intra-P pores within quartz show triangle and slit shapes (Figure 2I). OM pores in these samples can contribute to 60%–90% of total surface porosity (Table 1). Additionally, Table 1 shows that the mean size of OM pores in the Longmaxi shale ranges from 34 to 37 nm, whereas the mean size of mineral-associated pores is in the range of 55–85 nm. For the Qiongzhusi shale, the mean size of OM pores is about 29 nm, whereas the mean size of mineral-associated pores is about

TABLE 1 PCAS processing results.

Formation	Sample	Depth/m	Total surface porosity/%	Pore type	Surface porosity/%	Pore size/nm		Form factor	Probability entropy
						Max.	Ave.		
Longmaxi	C4	7143	3.19	OM pores	4.95	657	37	0.64	0.966
				Mineral-associated pores	0.27	2270	85	0.54	0.821
	C7	7149	2.50	OM pores	6.05	502	34	0.65	0.969
				Mineral-associated pores	0.19	525	55	0.54	0.742
Qiongzhusi	C26	8110	2.78	OM pores	5.51	414	29	0.61	0.946
				Mineral-associated pores	0.35	211	26	0.55	0.801
	C28	8127	1.80	OM pores	3.37	535	29	0.60	0.928
				Mineral-associated pores	1.02	654	57	0.53	0.898
	M18	7940	1.25	OM pores	0.26	203	75	0.58	0.813
				Mineral-associated pores	1.31	976	110	0.53	0.956

26–57 nm. The probability entropy of OM pores in all cases is close to 1, whereas that of mineral-associated pores ranges from 0.742 to 0.898, demonstrating that the mineral-associated pores are more directional than OM pores. Moreover, higher form factor values in OM pores indicate that they are more regular in shape compared with mineral-associated pores (Table 1).

Pore volume, specific surface area, and average pore diameter

The DFT method based on CO_2 and N_2 adsorption isotherms is a suitable method for exploring pores with sizes ranging from 0.33 to 100 nm (Thommes et al., 2006; Zhang et al., 2017). In this study, the DFT method for CO_2 and N_2 adsorption data was used to investigate the nanopore structure characteristics of the Longmaxi shale and Qiongzhusi shale from wells MS#1 and CS#1, and the calculated PV and SSA results are presented in Supplementary Table S2. The PV values derived from N_2 adsorption ($PV_{N2\text{-}DFT}$) in the Longmaxi and Qiongzhusi shale from well MS#1 are in the range of 0.0234–0.0356 cm^3/g (average 0.0289 cm^3/g) and 0.0272–0.0439 cm^3/g (average 0.0379 cm^3/g), respectively. Their SSA values derived from N_2 adsorption ($SSA_{N2\text{-}DFT}$) are in the range of 7.80–11.00 m^2/g (average 9.31 m^2/g) and 8.58–14.94 m^2/g (average 12.44 m^2/g), respectively. For the samples from CS#1, the $PV_{CO2\text{-}DFT}$ values for Longmaxi and Qiongzhusi shale range from 0.0021 to 0.0027 cm^3/g (average 0.0024 cm^3/g) and 0.0009–0.0022 cm^3/g (average 0.0016 cm^3/g), respectively, whereas their $SSA_{CO2\text{-}DFT}$ values are 15.76–17.38 m^2/g (average 16.31 m^2/g) and 9.40–15.26 m^2/g (average 12.27 m^2/g), respectively. In addition, the $PV_{N2\text{-}DFT}$ values for the Longmaxi and Qiongzhusi shale from well CS#1 are in the range of 0.0225–0.0453 cm^3/g (average 0.0299 cm^3/g) and 0.0058–0.0434 cm^3/g (average 0.0240 cm^3/g), respectively, whereas the $PV_{N2\text{-}DFT}$ values of these shales range from 13.03 to 17.20 m^2/g (average 14.69 m^2/g) and 2.41–16.02 m^2/g (average 9.46 m^2/g), respectively.

The APD derived from the N_2 adsorption isotherm was also obtained (Supplementary Table S2). The APD of the Longmaxi and Qiongzhusi shale from well MS#1 ranges from 15.73 to 20.37 nm (average 17.91 nm) and 11.92–21.46 nm (average 15.88 nm), respectively. Meanwhile, the APD of samples from well CS#1 is in the range of 8.75–14.09 nm (average 11.44 nm) and 9.45–15.04 nm (average 12.83 nm), respectively.

The ratios of mesopore/micropore volume (Me/MiPV) and mesopore/micropore surface area (Me/MiSSA), derived from N_2 adsorption data, are suitable parameters for describing the pore structure of ultra-deep shales (Jiao et al., 2018). The results of Me/MiPV and Me/MiSSA ratios for the samples are presented in Supplementary Table S2. The ratio of Me/MiPV of the Longmaxi and Qiongzhusi shale from well MS#1 is in the range of 16.93–24.44 (average 20.26) and 13.47–25.22 (average 18.95), respectively, whereas their Me/MiSSA ratio ranges from 2.33 to 2.98 (average 2.60) and 1.73–3.25 (average 2.47), respectively. For the samples from well CS#1, the Me/MiPV ratio of the Longmaxi and Qiongzhusi shales is 4.78–17.34 (average 8.72) and 6.05–37.49 (average 13.79), respectively, whereas their Me/MiSSA ratio is in the range of 0.72–2.55 (average 1.32) and 1.14–7.57 (average 2.54), respectively.

Multifractal characteristics

Multifractal analysis based on CO_2 and N_2 adsorption isotherms is a more suitable method for characterizing the multifractal characteristics of micropores and meso-macropores (Liu, 2018). In general, a non-linear correlation between $\tau(q)$ and q indicates the existence of fractal characteristics (Liu, 2018). Therefore, a non-linear correlation between $\tau(q)$ and q in our samples (Supplementary Figures

S1A–C) indicates that all shale samples have multifractal characteristics in their pores.

Supplementary Figures S1E, F demonstrate that D_q decreases rapidly with an increase of q, while $q < 0$ and D_q decrease slowly with an increase of q, where $q > 0$. The decreasing trend of D_q indicates the non-uniformity degree of micropores, mesopores, and macropores in shales. The multifractal parameters of all samples are shown in Supplementary Table S3. Among them, values of ΔD and H are widely used to characterize the connectivity and heterogeneity of shale pores (Liu et al., 2019). The ΔD value derived from the CO_2 adsorption isotherm (ΔD_{CO2}) of Longmaxi and Qiongzhusi shale from well CS#1 is in the range of 1.08–1.23 (average 1.17) and 0.59 to 1.47 (0.95), respectively, whereas their H values derived from the CO_2 adsorption isotherm (H_{CO2}) range from 0.88 to 0.90 (average 0.89) and 0.88–0.92 (average 0.89), respectively.

The ΔD_{N2} values of Longmaxi and Qiongzhusi shale from well MS#1 are 1.39–1.86 (average 1.66) and 1.23–1.89 (average 1.63), respectively, whereas their H_{N2} values range from 0.75 to 0.79 (average 0.78) and 0.76 to 0.85 (average 0.80), respectively. For the samples from well CS#1, the ΔD_{N2} values of Longmaxi and Qiongzhusi shale are in the range of 0.89–1.43 (average 1.24) and 0.83 to 1.71 (average 1.29), respectively. Meanwhile, their H_{N2} values range from 0.77 to 0.84 (average 0.80) and 0.65 to 0.86 (average 0.81), respectively.

Discussion

Differences in pore characteristics of shales from wells MS#1 and CS#1

We compare the Longmaxi and Qiongzhusi shale from well MS#1 and CS#1 to better understand the effects of pressure coefficient and shale burial depth on pore characteristics because the two wells are ultra-deep and have obvious differences in pressure coefficients.

1) There are some similarities in the two shales. For example, all samples in over-6000-m ultra-deep shale reservoirs show higher APD and Me/MiSSA values and higher Me/MiPV values compared to non-superdeep shales (Jiao et al., 2018). Moreover, type IV and H3 hysteresis loop patterns of the N_2 adsorption isotherm were observed in our samples (Supplementary Figure S2).
2) More pores (especially OM pores) are developed in the Longmaxi and Qiongzhusi shale from well CS#1 based on SEM observation, compared to those of well MS#1, indicating that the shales in well CS#1 may have better OM pore-preservation conditions. The OM pores are more regular than the mineral-associated pores, as mentioned previously, which means that the surfaces of OM pores are more complex. Generally, the surfaces of OM pores show harbor-like shapes, whereas the surfaces of mineral-associated pores are smooth (Figures 2E, F). Interestingly, the OM pores have many higher values of probability entropy compared to mineral-associated pores for the two shales from well CS#1, whereas the mineral-associated pores show higher values of probability entropy for the shales from well MS#1 (Table 1). This may indicate that mineral-associated pores in ultra-deep shales are easily compacted under over-pressure conditions, compared to OM pores, because the OM pores likely contain large amounts of gas to maintain their over-pressure. In normal pressure conditions, extremely strong compaction can lead to orientation of OM pores in ultra-deep shale. Meanwhile, many microfractures are generated among minerals with no discernible orientation, further resulting in a decrease in probability entropy.

The Longmaxi shale and Qiongzhusi shale are at the over-mature stage and contain a high TOC, indicating that they have considerable shale gas generation potential. A consensus was reached that silica minerals like quartz can provide a supporting framework for the preservation of OM pores (Clarkson et al., 2013; Cao et al., 2022), whereas carbonate cementation can reduce the PV of shale reservoirs (Zheng et al., 2018; Zheng et al., 2022). Quartz is very common in our samples, especially in the Longmaxi shales from well CS#1 (average 63.7%). OM pores are mainly distributed in pyrobitumen surrounded by quartz for the two shales from well CS#1 (Figures 2E, F), suggesting that quartz can protect these OM pores from compaction. For example, a high-quartz sample (C7) has the highest OM pore surface porosity, 6.05%, whereas the lower-quartz samples C26 and C28 have lower OM pore surface porosity (5.51% and 3.37%), despite their similar TOC contents, and are in over-pressure conditions (Supplementary Table S1). This indicates that shales with higher quartz have better pore preservation conditions.

Despite the similar hydrocarbon generation potentials and quartz content, the shales from well CS#1 were found to have higher OM-pore surface porosity than the shales from well MS#1. For example, the samples M18 and C26 have similar TOC values and quartz contents (Supplementary Table S1); however, the latter has a higher surface porosity for OM pores (Table 1). The current results of shale gas exploration and development in the Sichuan Basin show that the pressure coefficient can be used as a good indicator of the preservation condition of shale gas (Guo and Zhang, 2014). A higher pressure coefficient generally indicates better preservation (Gao et al., 2019; Wang et al., 2020). Therefore, pressure coefficient seems to be the main factor for OM pore preservation because the pressure coefficients of the two shales from well CS#1 (1.77–1.89) are higher than those of the shales from well MS#1 (1.01–1.46); that is, well CS#1 has better OM pore preservation than well MS#1. This further indicates that the differences in the development of OM pores within shales from wells MS#1 and CS#1 are mainly controlled by the pressure coefficient and quartz content. In addition, carbonate cementation has little effect on OM pore development in our shale samples due to their low carbonate content (average 9.30%) (Zheng et al., 2022).

3) The APD values of the Longmaxi and Qiongzhusi shale in our samples are much higher than in previous studies showing that the APD value of shallow-buried shales ranges from 3–7 nm (Hou et al., 2014; Jiao et al., 2018). Statistical results show that the APD value of most gas-producing shales generally ranges from 3 to 7 nm (Xie, 2020). The APD value of our samples is in the range of 8.75–21.46 (average 14.51 nm). Specifically, the APD values of the Longmaxi and Qiongzhusi shale from well CS#1 range from 8.75 to 14.09 nm (average 11.44 nm) and 9.45–15.98 nm (average 12.83 nm), respectively, which is lower than the Longmaxi (15.73–20.37 nm, average 17.91 nm) and Qiongzhusi shale (11.92–21.46 nm, average 15.88 nm) from well MS#1 (Figure 3). The results of PCAS processing show that the size of mineral-associated pores is much higher than that of OM pores. Notably,

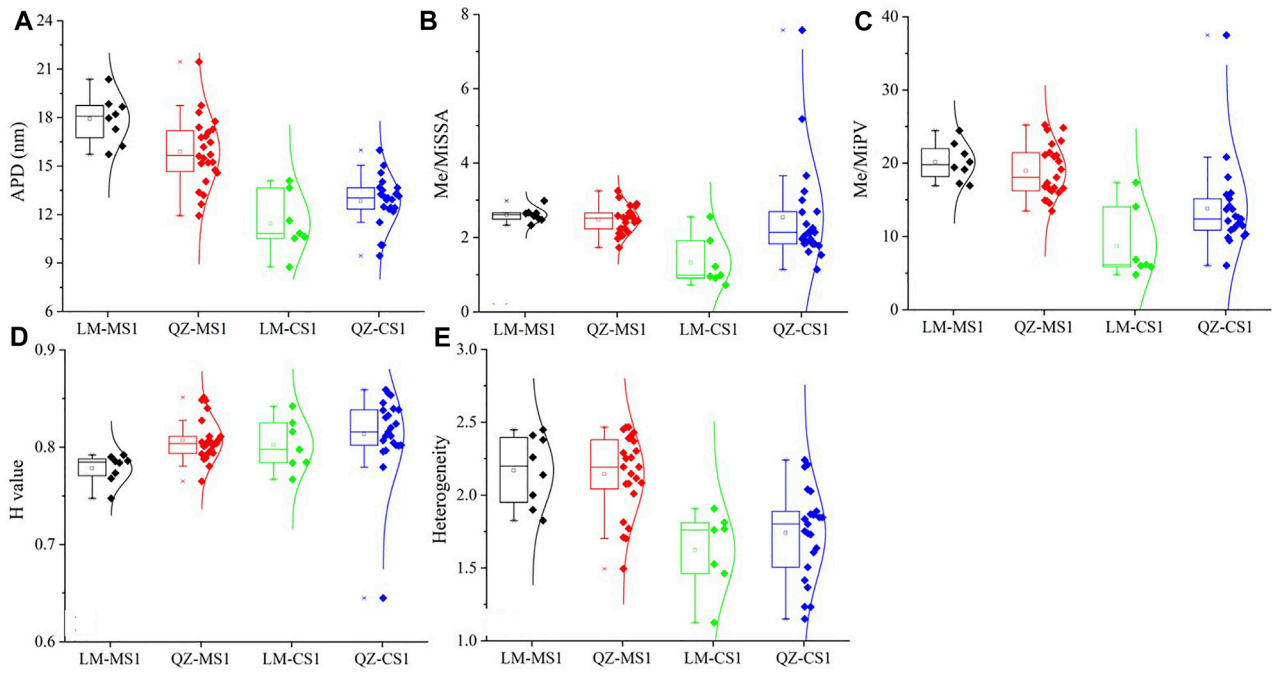

FIGURE 3
Comparison of pore structural parameters including **(A)** APD, **(B)** Me/MiSSA, **(C)** Me/MiPV, **(D)** H value and **(E)** Heterogeneity of shale samples.

the APD value of the Longmaxi shale is clearly smaller than that of the Qiongzhusi shale, whether from well CS#1 or MS#1, indicating that the OM pores with smaller sizes are easily developed in Longmaxi shale. Therefore, it is reasonable to believe that the smaller pore size of the Longmaxi shale is due to the development of OM pores.

4) The PSD of pores in over-6000-m ultra-deep shale reservoirs is characterized by multiple peaks (Supplementary Figure S3), which is different from previous studies showing that bimodal peaks are dominant in shallow shale reservoirs (Jiao et al., 2018). In addition, the ratios of Me/MiSSA and Me/MiPV in our samples exceed 1 and 5 (Figure 3). In addition, the ratios of Me/MiPV for the Longmaxi and Qiongzhusi shale in well MS#1 are significantly higher than those in well CS#1, implying that the two shales in well MS#1 have higher mesopore proportions. Therefore, we suggest that the high proportion of mesopores is a common feature of ultra-deep shale reservoirs.

Potential factors influencing pore connectivity and heterogeneity

CO_2 adsorption is a suitable method for studying the micropore range of pore size of organic-rich shales (0.33–2 nm), whereas N_2 adsorption can be used to characterize the wide range of pore sizes (2–200 nm) (Zhang et al., 2017; Jiao et al., 2018; Liu et al., 2019). Thus, multifractal analysis based on CO_2 and N_2 adsorption isotherms was used to study the connectivity and heterogeneity of micropores and meso-macropores (2–200 nm).

The heterogeneity comparison of micropores and meso-macropores in samples from well CS#1 shows that micropores have lower heterogeneity and higher H values as compared with meso-macropores (Supplementary Figures S4A, B). Moreover, no clear correlation is obtained between the micropore connectivity and meso-macropore connectivity of the two shales (Supplementary Figures S4C, D), indicating that the connectivity of shale micropores and meso-macropores needs to be studied separately.

The influence of PV and SSA

The correlation of PV, SSA, and the ΔD and H values of shales from well CS#1 is plotted in Figure 4 to determine whether pore structure parameters affect the heterogeneity and connectivity of pores. Figure 4A shows that there is a moderate positive correlation between ΔD value and micropore volume, whereas a moderate negative relationship is obtained between micropore volume and H value. This indicates that micropores in shale can increase the heterogeneity and reduce the connectivity of pores. Therefore, we inferred that the micropores in these samples may be widely distributed within the micropore aperture range. Remarkably, similar linear relationships are observed between the SSA of micropores and the ΔD and H values (Figure 4B). Notably, no obvious correlation is obtained between the PV and SSA of meso-macropores and the values of ΔD and H (Supplementary Figure S5), indicating that the meso-macropores have no obvious control over the heterogeneity and connectivity of pores in shale. This is consistent with the previous study by Liu (2018).

The influence of shale mineral composition

Given the difference in mineral composition, Pearson correlation analysis was performed to illustrate whether mineralogy or TOC could

10.3389/feart.2023.1059869

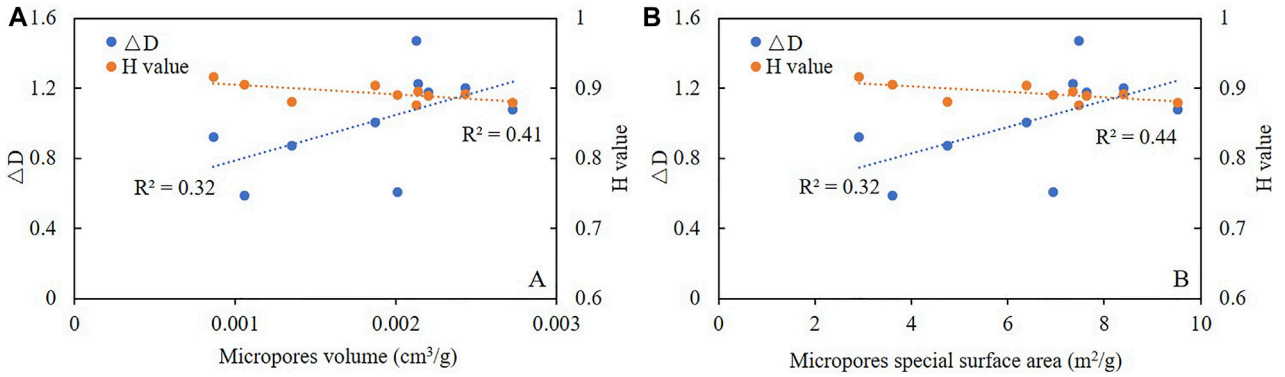

FIGURE 4
Correlation of micropores **(A)** and meso-macropore **(B)** volume and ΔD and H values.

TABLE 2 Relationship between mineral composition and values of △D and H for shales from well MS#1.

Parameter	TOC	Quartz	Feldspar	Calcite	Dolomite	Pyrite	Clays	$\Delta D_{Me\text{-}macro}$	$H_{Me\text{-}macro}$
TOC	1	0.09	.56**	−0.29	0.09	.74**	−.42*	0.16	0.18
Quartz		1	−0.01	−.72**	−.37*	−0.10	0.18	.46**	−.62*
Feldspar			1	−0.10	.42*	.62**	−.79**	0.08	0.24
Calcite				1	0.21	−0.11	−.39*	−0.22	.37*
Dolomite					1	.40*	−.47**	0.12	−0.07
Pyrite						1	−.65**	0.15	0.24
Clays							1	−0.15	−0.24
$\Delta D_{Me\text{-}macro}$								1	−.52**
$H_{Me\text{-}macro}$									1

Notes: * numbers indicate values > the critical correlation coefficient at the 95% significance level; ** numbers indicate values > the significant correlation coefficient at the 99% significance level.

TABLE 3 Relationship between mineral composition and values of △D and H for shales from well CS#1.

Parameter	TOC	Quartz	Feldspar	Calcite	Dolomite	Pyrite	Clays	ΔD_{Mi}	H_{Mi}	$\Delta D_{Me\text{-}macro}$	$H_{Me\text{-}macro}$
TOC	1	.50**	−0.27	−0.28	0.00	0.09	−0.34	0.26	0.30	−.42*	−0.12
Quartz		1	−.64**	−0.10	−0.09	−.51**	−.85**	0.62	−0.16	0.00	−0.05
Feldspar			1	−.46*	−.41*	.56**	0.35	−0.23	0.38	−0.04	0.17
Calcite				1	0.25	−0.25	0.12	−0.06	−0.51	0.26	−0.01
Dolomite					1	−0.32	0.02	−0.31	−0.35	−0.17	−.60**
Pyrite						1	.425*	−0.04	0.42	−0.06	0.05
Clays							1	−0.58	0.36	−0.06	0.19
ΔD_{Mi}								1	−0.39	−0.02	−0.39
H_{Mi}									1	−0.48	0.51
$\Delta D_{Me\text{-}macro}$										1	0.22
$H_{Me\text{-}macro}$											1

Notes: ditto.

control the pore heterogeneity and connectivity of shale. The quartz content of shales from well MS#1 is positively correlated with the ΔD value of meso-macropores, and a negative correlation between the quartz content and H value for meso-macropores was obtained (Table 2). This indicates that higher quartz content does lead to higher heterogeneity and lower connectivity for meso-macropores in shales from well MS#1. In addition, the calcite content is positively correlated with the H value of meso-macropores (Table 2), also indicating a higher connectivity of shale meso-macropores with high calcite content.

The correlation between mineral composition and ΔD and H values of micropores and meso-macropores in the two shales from well MS#1 differs from those from well CS#1 (Table 3). The TOC content is negatively correlated with the ΔD value of meso-macropores. This negative correlation also holds for the dolomite content *versus* H value of meso-macropores (Table 3). This indicates that lower TOC content can lead to less heterogeneity in meso-macropores and that higher dolomite content does lead to less connectivity of meso-macropores.

The quartz content has no obvious correlation with TOC, implying that quartz in shales from well MS#1 may be terrigenous. The effect of terrigenous quartz on the preservation of pores mainly provides a rigid framework to resist compaction and deformation (Thyberg et al., 2010; Ye et al., 2022). The dominance of mineral-associated pores in these shales (Table 1) indicates that these pores have relatively poor connectivity and further increases the heterogeneity of meso-macropores. The calcite content in the shales is in the range of 0%–21.1% (average 7.81%), and dissolved pores are observed within them. Notably, these dissolved pores are not filled with pyrobitumen, indicating that they may form after the generation of amounts of oil and gas and may be caused by the leaching of meteoric water. Therefore, these dissolved pores are conducive to increasing the connectivity of meso-macropores.

OM pores are profound and ubiquitous in shales from well CS#1 (Figures 2E, F), and they are mainly 20–250 nm, based on SEM observation. Therefore, the increase of TOC content can reduce the heterogeneity of meso-macropores because of their concentrated distribution. Carbonate cementation in carbonate-rich shale (carbonate content >10%) is common (Zheng et al., 2018; Zheng et al., 2022). Because of the extensive carbonate dissolution and subsequent re-precipitation, amounts of primary inter-P pores in carbonate-rich shale samples can be filled with carbonate cements. For example, high-carbonate sample C13 (calcite 6%, dolomite 21%) and sample C30 (calcite 4%, dolomite 19%) show much lower H values. This indicates that shales with higher carbonate content (including calcite and dolomite) have poorer pore connectivity.

Preservation mechanism of pores in over-6000-m ultra-deep shale reservoirs

The abundance of OM in shales is an important factor affecting pore development (Mastalerz et al., 2013; Zheng et al., 2022). Zheng et al. (2022) reported that with increasing TOC content, the PV of micropores, mesopores, and macropores in shales clearly increases. This phenomenon has been observed in our samples from well MS#1. A weakly positive relationship between TOC content and the PV and SSA of meso-macropores is obtained (Figure 5). The SEM images show that only a few OM pores are developed in these shales (Figures 2B, C). It is also clear that the OM in shales from well MS#1 contains more mesopores than macropores (Figure 2C). In addition, an obvious negative correlation between TOC content and the PV and SSA of meso-macropores in shales from well CS#1 is obtained (Figures 5B, C). This is quite distinct from previous studies (Zheng et al., 2018; Zheng et al., 2022). Milliken et al. (2013) and Zheng et al. (2022) reported that Devonian Marcellus shale and Silurian Longmaxi shale samples with TOC >5.5% demonstrate little or no contribution to the porosity of shale reservoirs with increasing TOC content. The ultra-deep Longmaxi shale and Qiongzhusi shale from well CS#1 suffered strong compaction. OM in ultra-deep burial is plastic mineral and susceptible to compaction at high temperature and pressure; this is why OM pore surface porosity in ultra-deep shale is clearly lower than in shallow-deep shale reservoirs (Xie, 2020). The negative correlation between TOC content and the PV and SSA of meso-macropores of the shale reservoir from well CS#1 also indicates this. Notably, the shale samples with TOC <2.0% contain many more PV of meso-macropores than those with TOC exceeding 2.0%, which does not accord with our SEM images showing that many OM pores are developed (Figures 2D, E). A careful comparison shows that the shale samples with high TOC content and low PPV and SSA all are from the Lower Qiongzhusi Formation (samples C23–C30). As is known, the direct floor of the Qiongzhusi Formation is a karst reservoir of the Late Sinian Dengying Formation that consists of dolomite, and the Tongwan unconformity between the Dengying Formation and Qiongzhusi Formation is widely distributed in most areas of the Sichuan Basin (Liu et al., 2021a). The Tongwan unconformity is an important channel for hydrocarbon migration in the Lower Paleozoic strata of the Sichuan basin (Liu et al., 2015; Liu et al., 2021a). The CS#1 well area is located on the eastern side of the Mianyang–Changning sag, and the efficiency of hydrocarbon emission is high (Liu et al., 2021a; Liu et al., 2021b). Thus, the Qiongzhusi shale close to the Tongwan unconformity is hard to maintain in over-pressure conditions, leading to decreasing pore size and further decreasing the PV and SSA of the shale reservoir. For the shales from well MS#1 close to the Tongwan unconformity, the PV and SSA are similar to the other samples. Consequently, the direct floor of the Qiongzhusi shale is an important factor controlling pore preservation in shale. After this factor was excluded, we found that TOC content is positively correlated with the PV of meso-macropores of shale with TOC <2.5%, whereas shale samples with TOC >2.5% show obvious decreases in meso-macropores with further increases in TOC (Figure 5C).

OM maturity is of great significance in the formation and development of pores, especially for OM pores (Curtis et al., 2012a; Curtis et al., 2012b; Zhang et al., 2020). Previous studies showed that Longmaxi shale has higher PV, SSA, and total porosity than Qiongzhusi shale and that Longmaxi shale has better pore connectivity (Zhang et al., 2020). The Longmaxi shale in this study has lower OM maturity compared to the Qiongzhusi shale, which shows much higher PV, SSA, and surface porosity. Marine shale reservoirs in the Sichuan Basin with ER_o ranging from 2.0% to 3.5% have considerable shale gas generation potential (Xie, 2020; Zheng et al., 2022). This further suggests that the differences in pore development (especially in OM pores) between the Longmaxi and Qiongzhusi shales and between the two wells have other, more important, causes than OM maturity.

Overall, geological factors affecting the pore development between the two shales and between the two wells can be summarized as follows.

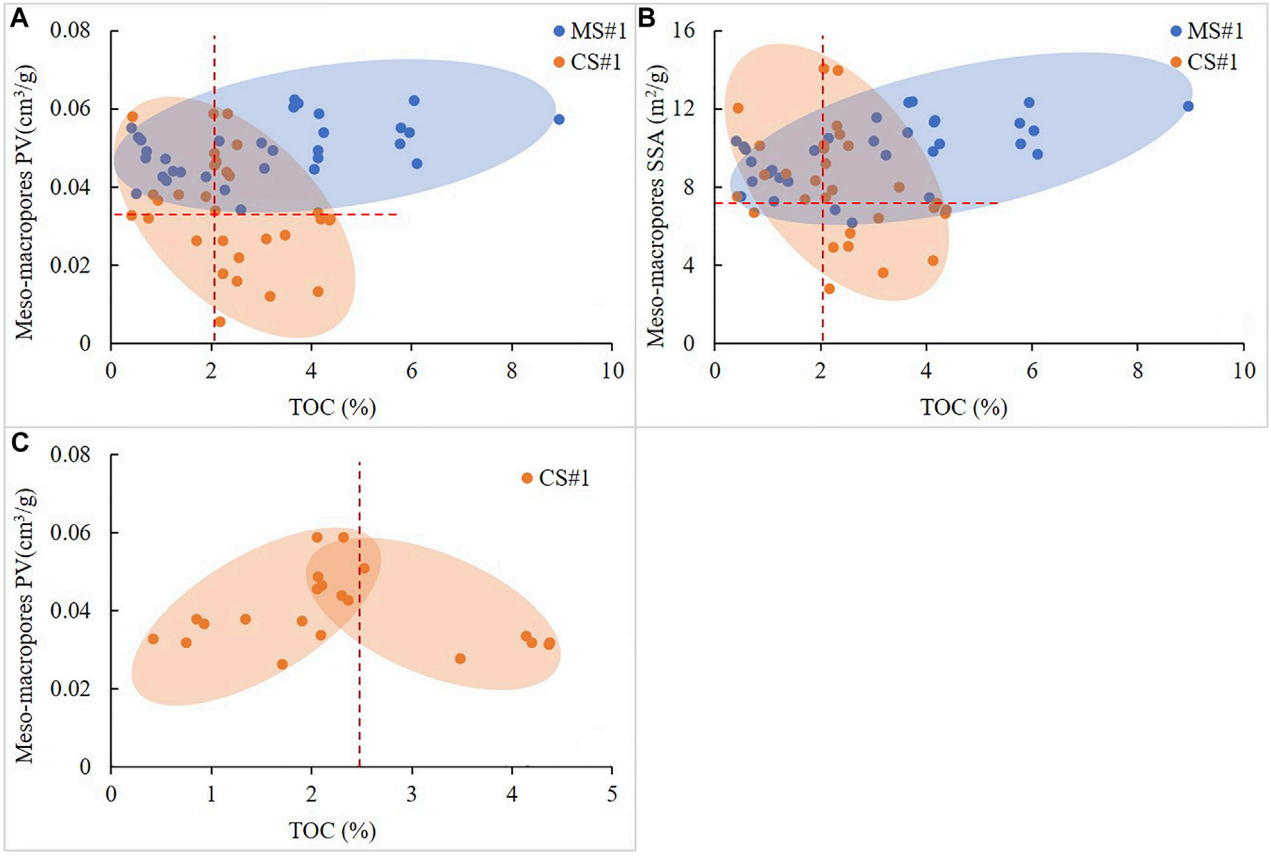

FIGURE 5
Relationship between TOC content and PV and SSA of meso-macropores of shales.

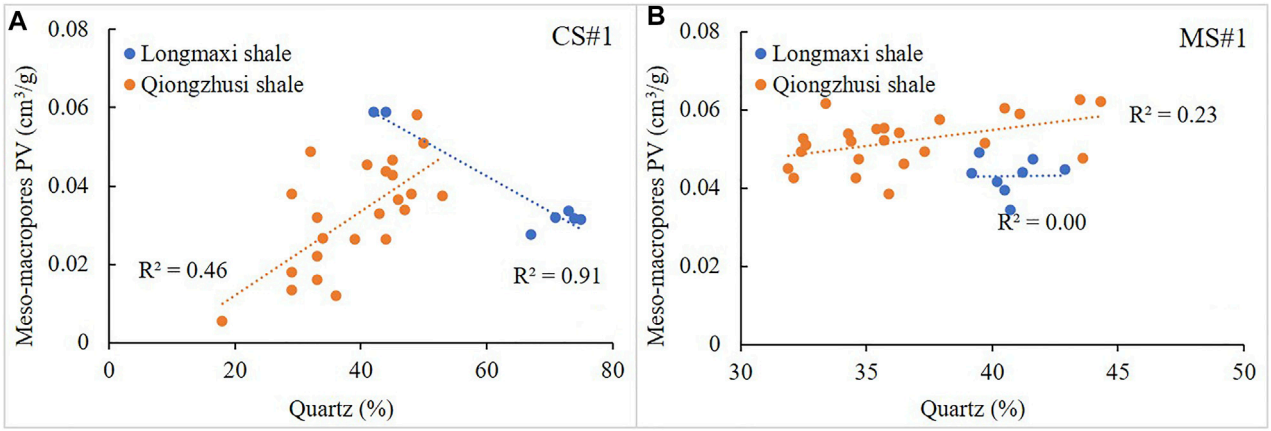

FIGURE 6
Correlation between quartz content and PV of meso-macropores. **(A)** CS#1 well; **(B)** MS#1 well.

1) The differences in the mineral composition and floor between the Longmaxi and Qiongzhusi shales are likely the critical factors controlling pore preservation. FE-SEM images show that OM pores are usually developed in shales with high quartz content (e.g., C4 and C7). A positive relationship exists between the PV of mesopores and quartz content for the Qiongzhusi shales from well CS#1 (Figure 6A). This is consistent with previous findings that quartz is conducive to the development of pores, especially OM pores (Dong et al., 2021; Guan et al., 2021). Notably, quartz content is negatively correlated with the PV of meso-macropores for the

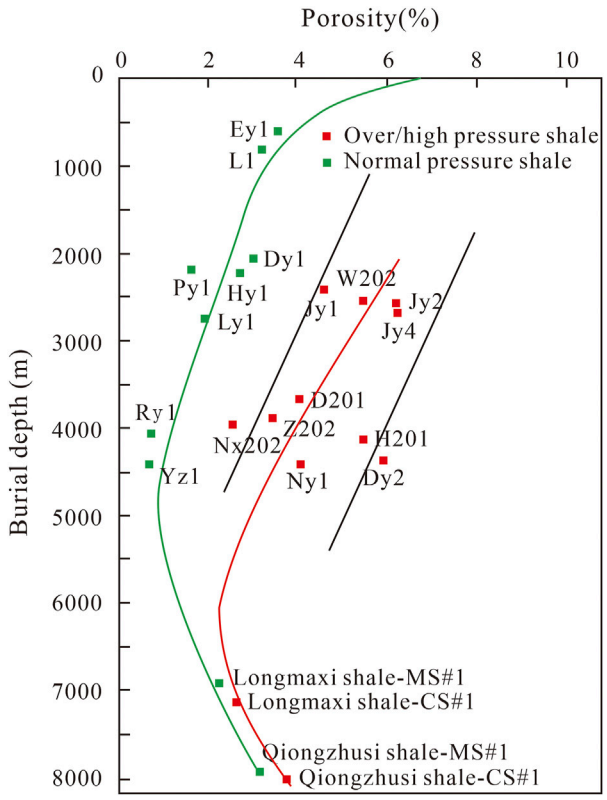

FIGURE 7
Relationship between porosity of the shale reservoir and burial depth.

Longmaxi shale from well CS#1 (Figure 6A), which is not in accordance with SEM observation. Further analysis showed that the samples with low PV of meso-macropores have high TOC content (e.g., C3–C7). Shales with high TOC content (>5%) are not favorable for the preservation of pores (Milliken et al., 2013). Interestingly, the relevance of quartz content and meso-macropore PV for shales from well MS#1 is very weak (Figure 6B), showing the obvious differences in pore structure of shales between the two wells. In addition, the floor of shale is critical for pore preservation, especially in the lower Qiongzhusi Formation, as mentioned previously.

2) The difference in the coefficient of shale between wells CS#1 and MS#1 is likely one such critical factor controlling pore development. Figure 3 shows obvious differences in pore structure, including the APD, Me/MiSSA, Me/MiPV, and H and ΔD values. In general, the shales from well MS#1 show higher APD values and higher proportions of mesopores, which do lead to greater heterogeneity. SEM observation showed that the shales from well CS#1 in over-pressure condition contain many more OM pores and have higher surface porosity than those from well MS#1 in normal pressure conditions (Xie, 2020). Statistics showed that the shales in over-pressure or high-pressure conditions have higher porosity than those in normal pressure conditions at different burial depths (Figure 7). Therefore, we have reason to believe that the coefficient of shale is the critical factor controlling the pore preservation in over-6000-m ultra-deep shale reservoirs.

Implications for deep-shale gas exploration

A better understanding of the pore preservation of ultra-deep shale may assist in the determination of favorable deep shale intervals and shale gas fields in the Sichuan Basin. Compared with Qiongzhusi shale, the higher quartz content (and the associated supporting effects) of the Longmaxi shales is one important factor positively affecting their pore development and preservation. In addition, the direct floor of the Qiongzhusi shale (and the associated Tongwan unconformity) is likely the critical geological factor negatively affecting their pore preservation and pressure coefficient and, ultimately, their gas contents. There is a threshold for the TOC content in shales, which favors OM pore development. The threshold of TOC is about 5.0% in shallow shale (Zheng et al., 2022) and even lower in deep shale reservoirs. Although the Qiongzhusi shale in the Sichuan Basin (MS#1) contains a high-quality shale interval of 80 m thickness, the low quartz content and Tongwan unconformity are not favorable for their pore preservation. Therefore, Longmaxi shale with both over-pressure or high pressure and high quartz content is likely the best target zone for deep shale gas exploration in the Sichuan Basin.

Conclusion

Samples from two ultra-deep wells, MS#1 and CS#1, were collected to study the pore characteristics and preservation mechanism of over-6000-m ultra-deep shale reservoirs in the Sichuan Basin. The conclusions are drawn as follows.

1) Ultra-deep shale reservoirs with burial depths of more than 6000 m have an obvious multifractal nature with different pore sizes. Compared with the two shales from well MS#1, the shales from well CS#1 contain relatively higher H values and lower ΔD values. This indicates that shale reservoirs in over-pressure conditions have better connectivity and less meso-macropore heterogeneity. Pearson correlation analysis indicated that quartz in the shales from well MS#1 can likely promote the preservation of pores (particularly mineral-associated pores in shales from well MS#1), further increase the heterogeneity of meso-macropores, and decrease the connectivity of meso-macropores. Meanwhile, calcite can increase the meso-macropore connectivity. In addition, for shales from well CS#1 with numerous bubble-like OM pores, TOC content can decrease meso-macropore heterogeneity. Calcite is conducive to increasing the meso-macropore connectivity of shales from well CS#1, particularly because the dissolved pores developed in these calcites are filled by pyrobitumen in OM pores.
2) The Longmaxi and Qiongzhusi shales in wells MS#1 and CS#1 have considerable shale gas generation potential because they contain high TOC contents and appropriate OM maturity. The Qiongzhusi shale in both wells, however, has relatively lower surface porosity and OM pore development degree than the Longmaxi shale. This further indicates that the surface porosity and development of OM pores are not only controlled by TOC contents and OM maturity but also by their quartz-supporting effect and pressure coefficient. Compared with Qiongzhusi shale, Longmaxi shale has a much higher quartz content and commonly has higher OM surface porosity and total surface porosity. The supportive effects of quartz seem to be a constructive factor that has promoted the preservation of OM pores. In addition, over-pressure conditions in the two shales in

well CS#1 likely lead to better OM pore preservation compared to those in well MS#1 that are under normal pressure conditions. Notably, the direct floor of the Qiongzhusi shale is also likely a critical geological factor affecting the pore structure and total surface porosity, and it seems to be a destructive factor that has decreased the PV and SSA of the shales. Based on this study, Longmaxi shale with both over-pressure or high-pressure conditions and high quartz content is likely the best target zone for deep-shale gas exploration in the Sichuan Basin.

Data availability statement

The original contributions presented in the study are included in the article/Supplementary Material; further inquiries can be directed to the corresponding authors.

Author contributions

GX and KJ designed the experiments and wrote the manuscript. BD performed the experiments. SL funded these experiments. WH and SL modified the manuscript. All authors contributed to the article and approved the submitted version.

Funding

This work was financially supported by the Natural Science Foundation of Anhui Province (Grant 2208085QD110), the National Natural Science Foundation of China (No. 42207293), the Key Scientific Research Foundation of the Education Department of the Province Anhui (No. 2022AH051748), the Key Programs of the Tongling University (No. 2021tlxyZD03), the Tongling University Starting Research Project (No. 2021tlxyrc16), and the Anhui University Excellent Research and Innovation Project (No. 2022AH010094). Natural Science Foundation of Sichuan Province (No. 2023NSFC0262).

Conflict of interest

The authors declare that the research was conducted in the absence of any commercial or financial relationships that could be construed as a potential conflict of interest.

Publisher's note

All claims expressed in this article are solely those of the authors and do not necessarily represent those of their affiliated organizations, or those of the publisher, the editors, and the reviewers. Any product that may be evaluated in this article, or claim that may be made by its manufacturer, is not guaranteed or endorsed by the publisher.

Supplementary material

The Supplementary Material for this article can be found online at: https://www.frontiersin.org/articles/10.3389/feart.2023.1059869/full#supplementary-material

References

Borjigin, T., Shen, B. J., Yu, L. J., Yang, Y. F., Zhang, W. T., Tao, C., et al. (2017). Mechanisms of shale gas generation and accumulation in the ordovician wufeng-longmaxi formation, Sichuan Basin, SW China. *Mar. Pet. Geol.* 44 (69), 69–78. doi:10.1016/s1876-3804(17)30009-5

Cao, T. T., Liu, H., Pan, A. Y., Fu, Y. T., Deng, M., Cao, Q. G., et al. (2022). Pore evolution in siliceous shales and its influence on shale gas-bearing capacity in eastern Sichuan-Western Hubei, China. *J. Pet. Sci. Eng.* 208, 109597. doi:10.1016/j.petrol.2021.109597

Chhabra, A., and Jensen, R. V. (1989). Direct determination of the f(α) singularity spectrum. *Phys. Rev. Lett.* 62, 1327–1330. doi:10.1103/PhysRevLett.62.1327

Clarkson, C. R., Solano, N., Bustin, R. M., Bustin, A. M. M., Chalmers, R. G. L., He, L., et al. (2013). Pore structure characterization of North American shale gas reservoirs using USANS/SANS, gas adsorption, and mercury intrusion. *Fuel* 103, 606–616. doi:10.1016/j.fuel.2012.06.119

Curtis, M. E., Cardott, B. J., Sondergeld, C. H., and Rai, C. S. (2012a). Development of organic porosity in the Woodford Shale with increasing thermal maturity. *Int. J. Coal Geol.* 103, 26–31. doi:10.1016/j.coal.2012.08.004

Curtis, M. E., Sondergeld, C. H., Ambrose, R. J., and Rai, C. S. (2012b). Microstructural investigation of gas shales in two and three dimensions using nanometer-scale resolution imaging. *AAPG Bull.* 96 (4), 665–677. doi:10.1306/08151110188

Dong, T., He, Q., He, S., Zhai, G. Y., Zhang, Y. R., Wei, S. L., et al. (2021). Quartz types, origins and organic matter-hosted pore systems in the lower cambrian Niutitang Formation, middle yangtze platform, China. *Mar. Pet. Geol.* 123, 104739. doi:10.1016/j.marpetgeo.2020.104739

Dyman, T. S., Wyman, R., Kuuakraa, V., Lewan, M., and Cook, T. A. (2003). Deep natural gas resources. *Nat. Resour. Res.* 12 (1), 41–56. doi:10.1023/A:1022656421803

Feng, Z. Q., Hao, F., Tian, J. Q., Zhou, S. W., Dong, D. Z., and Huang, S. (2022). Shale gas geochemistry in the Sichuan Basin, China. *Earth-Sci Rev.* 232, 104141. doi:10.1016/j.earscirev.2022.104141

Feng, G. X. (1988). Relationship between reflectance of bitumen and vitrinite in rock. *Nat. Gas. Ind.* 8 (8), 20–25. (In Chinese with English Abstract).

Gao, J., Zhang, J. K., He, S., Zhao, Z. L., He, Z. L., Wo, Y. J., et al. (2019). Over-pressure generation and evolution in Lower Paleozoic gas shales of theJiaoshiba region, China: Implications for shale gas accumulation. *Mar. Pet. Geol.* 102, 844–859. doi:10.1016/j.marpetgeo.2019.01.032

Gao, P., Xiao, X. M., Hu, D. F., Lash, G. G., Liu, R. B., Cai, Y. D., et al. (2022). Effect of silica diagenesis on porosity evolution of deep gas shale reservoir of the Lower Paleozoic Wufeng-Longmaxi formations, Sichuan Basin. *Mar. Pet. Geol.* 145, 105873. doi:10.1016/j.marpetgeo.2022.105873

Gou, Q. Y., Xu, S., Hao, F., Yang, F., Zhang, B. Q., Shu, Z. G., et al. (2019). Full-scale pores and micro-fractures characterization using FE-SEM, gas adsorption, nano-CT and micro-CT: A case study of the silurian Longmaxi Formation shale in the fuling area, Sichuan Basin, China. *Fuel* 253, 167–179. doi:10.1016/j.fuel.2019.04.116

Guan, Q. Z., Dong, D, Z., Zhang, H. L., Sun, S. S., Zhang, S. R., and Guo, W. (2021). Types of biogenic quartz and its coupling storage mechanism in organic-rich shales: A case study of the upper ordovician wufeng formation to lower silurian Longmaxi Formation in the Sichuan Basin, SW China. *Pet. Explor. Dev.* 48 (4), 813–823. doi:10.1016/S1876-3804(21)60068-X

Guo, T. L., and Zhang, H. R. (2014). Formation and enrichment mode of Jiaoshiba shale gas field, Sichuan Basin. *Pet. Explor. Dev.* 41 (1), 31–40. doi:10.1016/S1876-3804(14)60003-3

Guo, X. S., Hu, D. F., Li, Y. P., Wei, Z. L., Wei, X. F., and Liu, Z. J. (2017). Geological factors controlling shale gas enrichment and high production in Fuling shale gas field. *Pet. Explor. Dev.* 44 (4), 513–523. doi:10.1016/S1876-3804(17)30060-5

Halsey, T. C., Hensen, M. H., Kadanoff, L. P., Procaccia, I., and Shraiman, B. I. (1986). Fractal measures and their singularities: The characterization of strange sets. *Phys. R. A* 33 (2), 1141–1151. doi:10.1103/PhysRevA.33.1141

He, Z. L., Nie, H. K., and Jiang, T. X. (2021). Challenges and countermeasures of effective development with large scale of deep shale gas in Sichuan Basin[J]. *Reserv. Eval. Dev.* 11 (2), 1–11. (In Chinese with English Abstract).

Holmes, R., Rupp, E. C., Vishal, V., and Wilcox, J. (2017). Selection of shale preparation protocol and outgas procedures for applications in low-pressure analysis. *Energy fuels.* 31 (9), 9043–9051. doi:10.1021/acs.energyfuels.7b01297

Hou, Y. G., He, S., Yi, J. Z., Zhang, B. Q., Chen, X. F., Wang, Y., et al. (2014). Effect of pore structure on methane sorption capacity of shales. *Pet. Explor. Dev.* 41 (2), 248–256. doi:10.11698/PED.2014.02.17

Huang, H. X., Li, R. X., Jiang, Z. X., Li, J., and Chen, L. (2020). Investigation of variation in shale gas adsorption capacity with burial depth: Insights from the adsorption potential theory. *J. Nat. Gas Sci. Eng.* 73, 103043. doi:10.1016/j.jngse.2019.103043

Jiang, Z. X., Song, Y., Tang, X. L., Li, Z., Wang, X. M., Wang, G. Z., et al. (2020). Controlling factors of marine shale gas differential enrichment in southern China. *Pet. Explor. Dev.* 47 (3), 661–673. doi:10.1016/S1876-3804(20)60083-0

Jiao, K., Ye, Y. H., Liu, S. G., Ran, B., Deng, B., Li, Z. W., et al. (2018). Characterization and evolution of nanoporosity in superdeeply buried shales: A case study of the Longmaxi and Qiongzhusi shales from MS well #1, north Sichuan basin, China. *Energy fuels.* 32 (1), 191–203. doi:10.1021/acs.energyfuels.7b02932

Li, X. S., Zhu, H. J., Zhang, K. X., Li, Z., Yu, Y. X., Feng, X. Q., et al. (2021). Pore characteristics and pore structure deformation evolution of ductile deformed shales in the Wufeng-Longmaxi Formation, southern China. *Mar. Pet. Geol.* 127, 104992. doi:10.1016/j.marpetgeo.2021.104992

Liang, M., Wang, Z., Gao, L., Li, C. L., and Li, H. J. (2017). Evolution of pore structure in gas shale related to structural deformation. *Fuel* 197, 310–319. doi:10.1016/j.fuel.2017.02.035

Liu, C., Shi, B., Zhou, J., and Tang, C. S. (2011). Quantification and characterization of microporosity by image processing, geometric measurement and statistical methods: Application on SEM images of clay materials. *Appl. Clay Sci.* 54 (1), 97–106. doi:10.1016/j.clay.2011.07.022

Liu, K. Q., Ostadhassan, M., Sun, L. W., Zou, J., Yuan, Y. J., Gentzis, T., et al. (2019). A comprehensive pore structure study of the Bakken Shale with SANS, N_2 adsorption and mercury intrusion. *Fuel* 245, 274–285. doi:10.1016/j.fuel.2019.01.174

Liu, S. G., Yang, Y., Deng, B., Zhong, Y., Wen, L., Sun, W., et al. (2021a). Tectonic evolution of the Sichuan Basin, southwest China. *Earth-Sci Rev.* 213, 103470. doi:10.1016/j.earscirev.2020.103470

Liu, S. G., Li, Z. Q., Deng, B., Sun, W., Li, Z. W., Ding, Y., et al. (2021b). Occurrence morphology of bitumen in Dengying Formation deep and ultra-deep carbonate reservoirs of the Sichuan Basin and its indicating significance to oil and gas reservoirs[J]. *Nat. Gas. Ind.* 41 (8), 102–112. (In Chinese with English Abstract).

Liu, S. G., Sun, W., Zhao, Y. H., Wang, G. Z., Song, L. K., Deng, B., et al. (2015). Differential accumulation and distribution of natural gas and their maincontrolling factors in the Upper Sinian Dengying Fm, Sichuan Basin. *Natural Gas Industry* 35 (1), 10–23.

Liu, K. Q. (2018). *Microstructures and nanomechanical properties of the Bakken shale*. Grand Forks: University of North Dakota.

Lopes, R., and Betrouni, N. (2009). Fractal and multifractal analysis: A review. *Med. Image Anal.* 13, 634–649. doi:10.1016/j.media.2009.05.003

Loucks, R. G., Reed, R. M., Ruppel, S. C., and Jarvie, D. M. (2009). Morphology, genesis, and distribution of nanometer-scale pores in siliceous mudstones of the mississippian barnett shale. *J. Sediment. Res.* 79 (12), 848–861. doi:10.2110/jsr.2009.092

Loucks, R. G., Reed, R. M., Ruppel, S. C., and Hammes, U. (2012). Spectrum of pore types and networks in mudrocks and a descriptive classification for matrix-related mudrock pores. *AAPG Bulletin* 96 (6), 1071–1098. doi:10.1306/08171111061

Ma, Z. J., Tang, X., Deng, E. D., Liu, Y., Wang, Y. F., Zhang, J. Z., et al. (2022). Lithofacies and its controls on the organic matter-hosted pores in the Cambrian gas-rich Niutitang shale in upper Yangtze Plate, China. *J. Pet. Sci. Eng.* 218, 111052. doi:10.1016/j.petrol.2022.111052

Martínez, F. S., Martin, M. A., Caniego, F. J., Tuller, M., Guber, A., Pachepsky, Y., et al. (2010). Multifractal analysis of discretized X-ray CT images for the characterization of soil macropore structures. *Geoderma* 156, 32–42. doi:10.1016/j.geoderma.2010.01.004

Mastalerz, M., Schimmelmann, A., Drobniak, A., and Chen, Y. (2013). Porosity of devonian and mississippian new albany shale across a maturation gradient: Insights from organic petrology, gas adsorption, and mercury intrusion. *AAPG Bull.* 97 (10), 1621–1643. doi:10.1306/04011312194

Milliken, K. L., Rudnicki, M., Awwiller, D. N., and Zhang, T. W. (2013). Organic matter hosted pore system, Marcellus Formation (Devonian), Pennsylvania. *AAPG Bull.* 97 (2), 177–200. doi:10.1306/07231212048

Nie, H. K., Li, P., Dang, W., Ding, J. H., Sun, C. X., Liu, M., et al. (2022). Enrichment characteristics and exploration directions of deep shale gas of Ordovician-Silurian in the Sichuan Basin and its surrounding areas, China. *Pet. Explor. Dev.* 49 (4), 744–757. doi:10.1016/S1876-3804(22)60307-0

Paz-Ferreiro, J., Miranda, J. G. V., and Vidal Vázqueq, E. (2010). Multifractal analysis of soil porosity based on mercury injection and nitrogen adsorption[J]. *Vadose Zone J.* 9, 325–335. doi:10.2136/vzj2009.0090

Paz-Ferreiro, J., Da Luz, L. R. Q. P., Lado, M., and Vázquez, E. V. (2013). Specific surface area and multifractal parameters of associated nitrogen adsorption and desorption isotherms in soils from santa catarina, Brazil. *Vadose Zone J.* 6, vzj2012.0203–14. doi:10.2136/vzj2012.0203

Richardson, N. J., Densomore, A. L., Seward, D., Fowler, A., Wipf, M., Ellis, M. A., et al. (2008). Extraordinary denudation in the Sichuan Basin: Insights from lowtemperature thermochronology adjacent to the eastern margin of the Tibetan Plateau. *J. Geophys.l Res.* 113, B04409. doi:10.1029/2006JB004739

Shu, Y., Lu, Y. C., Chen, L., Wang, C., and Zhang, B. Q. (2020). Factors influencing shale gas accumulation in the lower Silurian Longmaxi formation between the north and South Jiaoshiba area, Southeast Sichuan Basin, China. *Mar. Pet. Geol.* 111, 905–917. doi:10.1016/j.marpetgeo.2019.06.029

Sing, K. S. W., Everett, D. H., Haul, R. A. W., Moscou, L., Pierotti, R. A., Rouquérol, J., et al. (1985). Physical and biophysical chemistry division commission on colloid and surface chemistry including catalysis. *Pure Appl. Chem.* 57, 6031–6036. doi:10.1351/pac198557040603

Soroushian, P., and Elzafraney, M. (2005). Morphological operations, planar mathematical formulations, and stereological interpretations for automated image analysis of concrete microstructure. *Compos* 27 (7-8), 823–833. doi:10.1016/j.cemconcomp.2004.07.008

Sun, M. D., Yu, B. S., Hu, Q. H., Chen, S., Xia, W., and Ye, R. C. (2016). Nanoscale pore characteristics of the lower cambrian niutitang formation shale: A case study from well yuke #1 in the southeast of chongqing, China. *Int. J. Coal Geol.* 154-155, 16–29. doi:10.1016/j.coal.2015.11.015

Teng, J., Liu, B., Mastalerz, M., and Schieber, J. (2022). Origin of organic matter and organic pores in the overmature ordovician-silurian wufeng-longmaxi shale of the Sichuan Basin, China. *Int. J. Coal Geol.* 2022, 103970. doi:10.1016/j.coal.2022.103970

Thommes, M., Smarsly, B., Groenewolt, M., Ravikovitch, P. I., and Neimark, A. V. (2006). Adsorption hysteresis of nitrogen and argon in pore networks and characterization of novel micro- and mesoporous silicas. *Langmuir* 22, 756–764. doi:10.1021/la051686h

Thyberg, B., Jahren, J., Winje, T., Bjørlykke, K., Faleide, J. I., and Marcussen, Ø. (2010). Quartz cementation in Late Cretaceous mudstones, northern North Sea: Changes in rock properties due to dissolution of smectite and precipitation of micro-quartz crystals. *Mar. Pet. Geol.* 27 (8), 1752–1764. doi:10.1016/j.marpetgeo.2009.07.005

Wang, H., He, Z. L., Zhang, Y. G., Bao, H. Y., Sun, K., Shu, Z. H., et al. (2019). Dissolution of marine shales and its influence on reservoir properties in the Jiaoshiba area, Sichuan Basin, China. *Mar. Pet. Geol.* 102, 292–304. doi:10.1016/j.marpetgeo.2018.12.017

Wang, M., Chen, Y., Bain, W., Song, G. Q., Liu, K. Y., Zhou, Z. Z., et al. (2020). Direct evidence for fluid over-pressure during hydrocarbon generation and expulsion from organic-rich shales. *Geology* 48, 374–378. doi:10.1130/G46650.1

Wang, E. Z., Guo, T. L., Li, M. W., Li, C. R., Dong, X. X., Zhang, N. X., et al. (2022). Exploration potential of different lithofacies of deep marine shale gas systems: Insight into organic matter accumulation and pore formation mechanisms. *J. Nat. Gas. Sci. Eng.* 102, 104563. doi:10.1016/j.jngse.2022.104563

Xi, Z. D., Tang, S. H., Zhang, S. H., Lash, G. G., and Ye, Y. P. (2022). Controls of marine shale gas accumulation in the eastern periphery of the Sichuan Basin, South China. *Int. J. Coal Geol.* 215, 103939. doi:10.1016/j.coal.2022.103939

Xie, G. L. (2020). *Pore structure characteristics of the Lower Paleozoic marine shale in the Sichuan Basin and their relationships with burial depth of shale*. Chengdu: Chengdu University of Technology.

Ye, Y. P., Tang, S. H., Xi, Z. D., Jiang, D. X., and Duan, Y. (2022). Quartz types in the Wufeng-Longmaxi Formations in southern China: Implications for porosity evolution and shale brittleness. *Mar. Pet. Geol.* 137, 105479. doi:10.1016/j.marpetgeo.2021.105479

Yu, K., Zhao, K. D., and Ju, Y. W. (2022). A comparative study of the permeability enhancement in coal and clay-rich shale by hydraulic fracturing using nano-CT and SEM image analysis. *Appl. Clay Sci.* 218, 106430. doi:10.1016/j.clay.2022.106430

Yu, Y. X., Wang, Z. X., Zhang, K. X., Feng, X. Q., and Cheng, M. (2022). Effects of shear on development characteristics of organic matter pores in shale: A case study of shale in the niutitang formation of the well XAD1. *J. Pet. Sci. Eng.* 211, 110166. doi:10.1016/j.petrol.2022.110166

Zhang, L., Xiong, Y. Q., Li, Y., Wei, M. M., Jiang, W. M., Lei, R., et al. (2017). DFT modeling of CO_2 and Ar low-pressure adsorption for accurate nanopore structure characterization in organic-rich shales. *Fuel* 204, 1–11. doi:10.1016/j.fuel.2017.05.046

Zhang, Y. F., Yu, B. S., Pan, Z. J., Hou, C. H., Zou, Q. W., and Sun, M. D. (2020). Effect of thermal maturity on shale pore structure: A combined study using extracted organic matter and bulk shale from Sichuan Basin, China. *J. Nat. Gas. Sci. Eng.* 74, 103089. doi:10.1016/j.jngse.2019.103089

Zheng, Y. J., Liao, Y. H., Wang, Y. P., Xiong, Y. Q., and Peng, P. A. (2018). Organic geochemical characteristics, mineralogy, petrophysical properties, and shale gas prospects of the Wufeng-Longmaxi shales in Sanquan Town of the Nanchuan District, Chongqing. *AAPG Bull.* 102 (11), 2239–2265. doi:10.1306/04241817065

Zheng, Y. J., Liao, Y. H., Wang, Y. P., Xiong, Y. Q., and Peng, P. A. (2022). The main geological factors controlling the Wufeng-Longmaxi shale gas content. *AAPG Bull.* 106 (10), 2073–2102. doi:10.1306/07132218243

Zhu, C. Q., Qiu, N. S., Jiang, Q., Hu, S. B., and Zhang, S. (2015). Thermal history reconstruction based on multiple paleo-thermal records of the yazihe area, western sichuan depression, SW China. *Chin. J. Geophys.* 58 (10), 599–610. doi:10.1002/cjg2.20198

Zou, C. N., Dong, D. Z., Wang, S. J., Li, J. Z., Li, X. J., Wang, Y. M., et al. (2010). Geological characteristics and resource potential of shale gas in China. *Pet. Explor. Dev.* 37 (6), 641–653. doi:10.1016/S1876-3804(11)60001-3

Zou, C. N., Dong, D. Z., Wang, Y. M., Li, X. J., Huang, J. L., Wang, S. F., et al. (2016). Shale gas in China: Characteristics, challenges and prospects (II). *Pet. Explor. Dev.* 43 (2), 182–196. doi:10.1016/S1876-3804(16)30022-2

Zou, C. N., Zhu, R. K., Chen, Z. Q., Ogg, J. G., Wu, S. T., Dong, D. Z., et al. (2019). Organic-matter-rich shales of China. *Earth-Sci Rev.* 189, 51–78. doi:10.1016/j.earscirev.2018.12.002